Nonlinear Dyn (2014) 76:1737–1751
DOI 10.1007/s11071-014-1242-3

ORIGINAL PAPER

Dynamics and control of a parallel mechanism for active vibration isolation in space station

Jinguo Liu · Yangmin Li · Yang Zhang · Qing Gao · Bin Zuo

Received: 24 August 2013 / Accepted: 4 January 2014 / Published online: 30 January 2014

Abstract Vibration in the microgravity environment is with the characteristics of low frequency, small amplitude, and randomness. Control method of an active vibration isolation system with parallel mechanism applied to space application, which is effective for disturbance suppression, is proposed. The dynamics model of active vibration isolation system with payload is represented via Kane's method, thereafter the description in state-space linearization is introduced. System properties and step responses of the systems in open loop are evaluated in detail. Controllability and observability of the system are checked by state-space equations of the system. The state feedback decoupling with double-loop proportional-integral-derivative (PID) control method is adopted as the system controller to design the decoupling matrix and the PID controller. For improving the properties of the system, a control system with H-infinity method is also designed and evaluated. Finally, various types of simulation results are demonstrated to verify the effectiveness of the active vibration damping system proposed.

Keywords Active vibration isolation · Space station · Control method · PID control · H_∞ control

J. Liu · Y. Li · Y. Zhang · Q. Gao · B. Zuo
State Key Laboratory of Robotics, Shenyang Institute of Automation, Chinese Academy of Sciences, Shenyang 110016, China
e-mail:liujinguo@sia.cn

Y. Li (✉)
Department of Electromechanical Engineering, University of Macau, Macao 999078, China
e-mail:ymli@umac.mo

Y. Li
School of Mechanical Engineering, Tianjin University of Technology, Tianjin 300384, China

Q. Gao · B. Zuo
University of the Chinese Academy of Sciences, Beijing 100049, China

1 Introduction

It is an effective way to take the advantages of the microgravity environment for making scientific experiments in the space station. However, due to the various types of sources producing vibration, various experimental conditions in the space station in terms of the varying acceleration are not ideal for scientific research. Taking the International Space Station (ISS) for example, its vibration sources are divided into three categories according to the frequency [1–5]: (a) low frequency less than 10^{-3} Hz, which is caused by gravity and atmospheric drag of orbital space; (b) high frequency larger than 1 Hz produced by continuing sources such as the vibrations of pumps, compressors, motors, and fans, as well as the movement of the crew and propeller, which appears as the transient source; (c) medium frequency between 10^{-3} and 1 Hz, which is caused by walking of the crew, propeller movement, etc. Sources producing vibration interference in space

station have the features of low frequency, small amplitude, and randomness. Thus, designing a damping system, which is effective for isolating the low-frequency interference sources in space station, is absolutely crucial to make space experiment accurately.

As required by experimental conditions in space station with microgravity environment, especially for that of the acceleration, a novel damping system should be designed. At present, there are four major international damping systems for space science experiments, named Suppression of Transient Acceleration by Levitation (STABLE), Active Rack Isolation System (ARIS), Microgravity Vibration Isolation Mount (MIM), and Glove box Integrated Microgravity Isolation Technology (G-LIMIT). Taking account for the size of the load, the damping system with space application is divided into three levels: payload level, the sub-cabinet level, and the whole cabinet level. STABLE and G-LIMIT are both payload level damping systems. STABLE utilized six independent controlled Lorentz coils to reduce vibration for suspending loads, while G-LIMIT used the glove box to conduct scientific experiments. MIM is damping system for the sub-cabinet level, which utilized eight Lorentz drives that are centralized control to resist vibration disturbances. Thus, a variety of scientific experiments can be performed [1–4]. ARIS is the damping system for the entire cabinet level, which uses sensors to measure acceleration signals of the experimental cabinet and controls the eight swing-type voice coil motors providing the driving force. With this solution, the whole experimental cabinet is isolated from low-frequency interference [4–10].

There are many key technologies of designing the parallel mode active damping system [11]: (a) design and optimize the system mechanism. Select the appropriate drive and reduce the direction of multi-freedom vibration interference by providing the driving force through the rational layout; (b) system design and layout of key components, such as flexure hinge design and distributing the sensors; and (c) design and optimize the control system.

Active damping system often uses double-loop control, which is an acceleration feedback and position feedback and is a multi-input multi-output system. The design of control system is divided into traditional control methods and modern control methods.

The main content of this paper is as follows: First of all, Kane's method is used to establish dynamics model of spatial cabinet parallel active isolation system and dynamics model of space station science experimental load; and the model is linearized to obtain the form of state-space model. Open-loop characteristics of the system are studied; and step response of the open-loop system is analyzed; then through systematic state-space equations, we analyzed the controllability and observability of the system. The methods of proportional-integral-derivative (PID) and H infinity (H_∞) are used to design control system. At last, the simulation experiments verify the damping effect of the designed active vibration isolation system.

2 Configuration of active isolation system for microgravity scientific research platform

The layout of the sensitive experiment payload in space station for scientific research is illustrated in Fig. 1. According to the isolation and damping mechanism of the International Space Station (ISS) and the requirements for attenuation of vibration, a novel active vibration isolation and damping system with parallel distributed isolators is designed, which is shown in Fig. 2. The main features of the proposed system are as following. First, it consists of three component elements, including the cabin of space station, the platform for scientific research, and the actuators which are taken as the isolators. Moreover, the platform for scientific research is mounted on cabin of the space station isolated via eight voice coil motors in parallel mechanisms through which the systematic rigidity and reliability are increased. Finally, there are no special requirements of the characteristics for voice coil motor, and the flexure

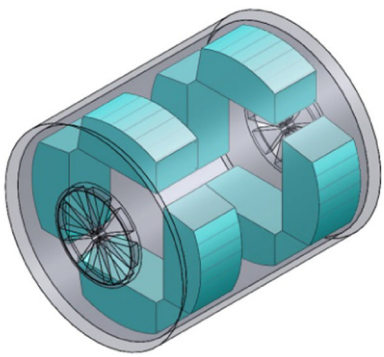

Fig. 1 Layout of the microgravity scientific research rack in the space station section

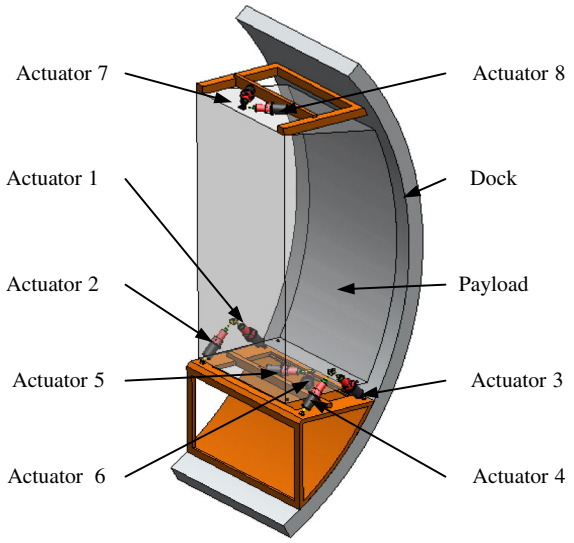

Fig. 2 The parallel active vibration isolation system of space station scientific experimental rack

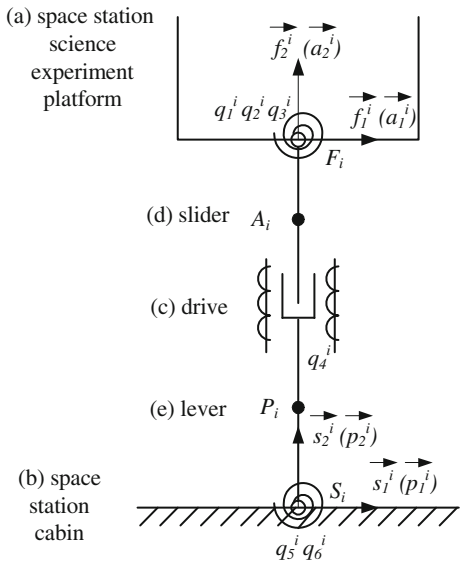

Fig. 3 The reference coordinate system

hinge is designed separately with the motor for system assembling considerations.

According to the formula of Kutazbach–Grübler, the degree of freedom (DOF) of the mechanism illustrated is derived from

$$M = 6\,(n - g - 1) + \sum_{i=1}^{g} f_i = 6, \tag{1}$$

where M represents the DOF and n is the number of the elements. The number of kinematic pairs is g, while f_i represents the relative DOF.

Various types of actuators are eligible for active vibration isolation system, such as piezoelectric ceramic (PZT), magnetostrictive materials, hydraulic cylinders, voice coil motor, etc. However, the performance of active vibration isolation system is highly relied on that of the driving components, thus the actuator is a critical component in an active vibration isolation system. Voice coil motor consists of coil elements and magnet elements. Considering different types of output, it is divided into two categories: the linear type and the sway type. Compared with other types of actuators, there are a lot of advantages of a voice coil motor, such as simplified structure, small size, larger acceleration, fast response, and high repeated resolution. Due to the proportional relation between the output of force and the input of current, it is effective for requirements of controlling the acceleration.

As the scientific research platform of the space station is sensitive for vibrations, it requires the actuator to output larger force rapidly with both good performance and robustness, besides a smaller size. Therefore, the proposed active isolation system utilizes the linear voice coil motors as the actuators, which are distributed in parallel.

3 Dynamics modeling of the active vibration isolation system

3.1 Coordinate system description for active isolation platform

Model of the active isolation system for microgravity scientific research is shown in Fig. 3, which consists of the following components: (a) microgravity scientific research platform, (b) cabin of the space station, and (c) several actuators. In this design, a single-axis actuator includes the slider (d) and the static lever (e). The slider is mounted on the microgravity scientific research platform via a 3-DOF flexure hinge, while the static lever is fixed on the cabin of the station through a 2-DOF flexure hinge. Thus, the slider could move linearly with respect to the static lever.

As illustrated in the model, the flexure hinge is simplified as spring with the mass neglected. The cabin of the space station is taken as the base, and the platform

for scientific research has 6 degrees of freedom which are driven by actuators. The primary position of the platform is defined as the position when all the springs are relaxed without any pressures. The center of mass of the space station cabin, the static lever, the slider, and the science experiment platform are represented by S^*, Pi^*, Ai^*, and Fi^*, respectively. The lengths of slider and static lever are l_1^i and l_2^i. Connection point between static lever and the cabin of space station is S^i, while that between slider and scientific experimental platform is F^i. The points of Lorentz force generated by the coil are A^i. The superscript * denotes the center of mass of each rigid elements, and superscript and subscript i denote the i-th actuator.

According to the original point F^i $(i = 1, \ldots, 8)$, eight groups of reference coordinate system $\widehat{F_i}$ are established on scientific experimental platform and the reference coordinate system is determined by the unit vector $\vec{f}_j^i$ $(j = 1, 2, 3)$. When the scientific experimental platform is at the initial position as shown in Fig. 3; $\vec{f}_2^i$ along the slider is perpendicular to the surface of the platform and $\vec{f}_1^i$ is perpendicular to $\vec{f}_2^i$, while $\vec{f}_1^i$ is parallel to the side of scientific experimental platform. Direction of $\vec{f}_3^i$ was determined by the right-hand rule $\vec{f}_1^i \times \vec{f}_2^i$, and it is perpendicular to side of the scientific experimental platform and pointing to the external.

Correspondingly, to the original point F^i, eight groups of reference coordinate systems $\widehat{A_i}$ on slider are also established and the position of reference coordinate system is determined by the unit vector $\vec{a}_j^i$ $(j = 1, 2, 3)$. Meanwhile, eight groups of reference coordinate systems $\widehat{P_i}$ on lever are shown in Fig. 3. The direction of reference coordinate system is determined by the unit vector $\vec{p}_j^i$ $(j = 1, 2, 3)$. After that, eight groups of reference coordinate system $\widehat{S_i}$ on the space station cabin are illustrated and the direction of reference coordinate system is determined by the unit vector $\vec{s}_j^i$ $(j = 1, 2, 3)$. While the scientific experiment platform is at the initial position, $\vec{a}_j^i$, $\vec{p}_j^i$, $\vec{s}_j^i$, and $\vec{f}_j^i$ have the same position. Finally, to the original point F^* of science experiment platform's initial position, establishing static coordinate system and the position of coordinate system are determined by the unit vector $\vec{f}_j$ $(j = 1, 2, 3)$, where $\vec{f}_1$, $\vec{f}_2$, and $\vec{f}_3$ point to the front, top, and side of platform for scientific experiments, respectively.

The rotations between $\vec{a}_j^i$ and $\vec{f}_j^i$ through $\vec{f}_1^i$, $\vec{f}_2^i$, and $\vec{f}_3^i$ are defined as q_1^i, q_2^i, and q_3^i, respectively. The transformations q_4^i between $\vec{p}_j^i$ and $\vec{a}_j^i$ are defined, while the rotation q_5^i and q_6^i through $\vec{s}_1^i$ and $\vec{s}_3^i$ between $\vec{s}_j^i$ and $\vec{p}_j^i$ are also shown in Fig. 3.

By defining the sine and cosine variants of q_j^i as c_j^i and s_j^i, respectively, the rotations between $\widehat{A_i}$ and $\widehat{F_i}$ as well as between $\widehat{P_i}$ and $\widehat{S_i}$ are solved as:

$$R_a^f = \begin{bmatrix} c_3^i c_2^i & c_3^i s_2^i s_1^i - s_3^i c_2^i & c_3^i s_2^i c_1^i + s_3^i s_1^i \\ s_3^i c_2^i & s_3^i s_2^i s_1^i + c_3^i c_1^i & s_3^i s_2^i c_1^i - c_3^i s_1^i \\ -s_2^i & c_2^i s_1^i & c_2^i c_1^i \end{bmatrix}, \quad (2)$$

$$R_p^s = \begin{bmatrix} c_6^i & -c_5^i s_6^i & s_5^i s_6^i \\ s_6^i & c_5^i c_6^i & -s_5^i c_6^i \\ 0 & s_5^i & c_5^i \end{bmatrix}. \quad (3)$$

3.2 Assumptions for simplified model

By attenuation of the amplitude of system vibration, active vibration isolation and damping system could keep the platform stable around the expected position. Due to the performance and characteristics of the active isolation system via parallel distributed isolators, several assumptions are conducted for this system as follows:

(a) All the transformations q_j^i and generalized velocities u_j^i are rather small;
(b) Nonlinear differential equation is approximately represented by the first-order differential equation;
(c) The angular velocities ω^S and the angular acceleration α^S are neglected, while those of linear movements are rather small.

3.3 Generalized velocity, partial velocity, and acceleration

There are totally 48 variants of $q_j^i (j = 1, \ldots, 6;\ i = 1, \ldots, 8)$, which include 42 representing angular properties and the other 6 representing variants for transformation, defined as generalized coordinates of the dynamics for $\tilde{S}$.

The first-order time derivative of generalized coordinate system u_j^i $(j = 1, \ldots, 6;\ i = 1, \ldots, 8)$ is given by

$$u_j^i = \dot{q}_j^i, \quad (4)$$

while $u_j^1 (j = 1, \ldots, 6)$ is selected as the independent generalized velocity.

Assuming that $\vec{r}^{AB}$ is the vector from A pointing to B, vectors in the proposed system are as follows:

$$\vec{r}^{S_i P_i^*} = p_2^i \vec{p}_2^i, \tag{5}$$
$$\vec{r}^{A_i^* F_i} = a_2^i \vec{a}_2^i, \tag{6}$$
$$\vec{r}^{P_i^* A_i^*} = p_2^i \vec{p}_2^i + q_4^i \vec{p}_2^i + a_2^i \vec{a}_2^i, \tag{7}$$
$$\vec{r}^{F_i F^*} = f_1^i \vec{f}_1^i + f_2^i \vec{f}_2^i + f_3^i \vec{f}_3^i, \tag{8}$$

where f_1^i, f_2^i, and f_3^i are correspondingly the projections of $\vec{f}_1^i$, $\vec{f}_2^i$, and $\vec{f}_3^i$, which represent the distances from F_i to the center of mass of the scientific platform F^*.

Velocity of the center of mass can be derived by time derivatives of the vectors of position. Thus, based on the assumptions aforementioned, the relations $\sin q_i = q_i$ and $\cos q_i = 1$ existed. After omitting the high-order minimum, the linear velocities are derived as:

$$\overset{S_i}{}_l \vec{v}^{P_i^*} = p_2^i \left(u_6^i \vec{s}_l^i - u_5^i \vec{s}_3^i \right), \tag{9}$$
$$\begin{aligned} \overset{S_i}{}_l \vec{v}^{A_i^*} &= u_4^i \vec{s}_2^i - u_5^i \left(a_2^i + l_2^i \right) \vec{s}_3^i \\ &\quad + u_6^i \left(a_2^i + l_2^i \right) \vec{s}_1^i, \end{aligned} \tag{10}$$
$$\begin{aligned} \overset{S_1}{}_l \vec{v}^{F^*} &= u_1^1 \left(-f_3^1 \vec{s}_2^1 + f_2^1 \vec{s}_3^1 \right) \\ &\quad + u_2^1 \left(f_3^1 \vec{s}_1^1 - f_1^1 \vec{s}_3^1 \right) \\ &\quad + u_3^1 \left(-f_2^1 \vec{s}_1^1 + f_1^1 \vec{s}_2^1 \right) \\ &\quad + u_4^1 \vec{s}_2^1 + u_5^1 \left[f_3^1 \vec{s}_2^1 - \left(f_2^1 + l_1^1 + l_2^1 \right) \vec{s}_3^1 \right] \\ &\quad + u_6^1 \left[\left(f_2^1 + l_1^1 + 1_2^1 \right) \vec{s}_1^1 - f_1^1 \vec{s}_2^1 \right]. \end{aligned} \tag{11}$$

Let $f_2^1 + l_1^1 + l_2^1 = h^1$; the equation above is transformed as

$$\begin{aligned} \overset{S_1}{}_l \vec{v}^{F^*} &= u_1^1 \left(-f_3^1 \vec{s}_2^1 + f_2^1 \vec{s}_3^1 \right) \\ &\quad + u_2^1 \left(f_3^1 \vec{s}_1^1 - f_1^1 \vec{s}_3^1 \right) \\ &\quad + u_3^1 \left(-f_2^1 \vec{s}_1^1 + f_1^1 \vec{s}_2^1 \right) \\ &\quad + u_4^1 \vec{s}_2^1 + u_5^1 \left(f_3^1 \vec{s}_2^1 - h^1 \vec{s}_3^1 \right) \\ &\quad + u_6^1 \left(h^1 \vec{s}_1^1 - f_1^1 \vec{s}_2^1 \right). \end{aligned} \tag{12}$$

Moreover, the linearized accelerations can be solved by the time derivatives of velocity of rigid body after linearization.

$$\overset{S_i}{}_l \vec{a}^{P_i^*} = p_2^i \left(\dot{u}_6^i \vec{s}_1^i - \dot{u}_5^i \vec{s}_3^i \right), \tag{13}$$
$$\begin{aligned} \overset{S_i}{}_l \vec{a}^{A_i^*} &= \dot{u}_4^i \vec{s}_2^i - \dot{u}_5^i \left(a_2^i + l_2^i \right) \vec{s}_3^i \\ &\quad + \dot{u}_6^i \left(a_2^i + l_2^i \right) \vec{s}_1^i, \end{aligned} \tag{14}$$
$$\begin{aligned} \overset{S_1}{}_l \vec{a}^{F^*} &= \dot{u}_1^1 \left(-f_3^1 \vec{s}_2^1 + f_2^1 \vec{s}_3^1 \right) \\ &\quad + \dot{u}_2^1 \left(f_3^1 \vec{s}_1^1 - f_1^1 \vec{s}_3^1 \right) \\ &\quad + \dot{u}_3^1 \left(-f_2^1 \vec{s}_1^1 + f_1^1 \vec{s}_2^1 \right) \\ &\quad + \dot{u}_4^1 \vec{s}_2^1 + \dot{u}_5^1 \left(f_3^1 \vec{s}_2^1 - h^1 \vec{s}_3^1 \right) \\ &\quad + \dot{u}_6^1 \left(h^1 \vec{s}_1^1 - f_1^1 \vec{s}_2^1 \right). \end{aligned} \tag{15}$$

Then, the partial velocities linearizations are obtained as follows.

(a) The linearization partial velocity of the static lever is

$$\overset{S_i}{}_l \vec{v}_r^{P_i^*} = \frac{\partial \overset{S_i}{}_l \vec{v}^{P_i^*}}{\partial u_r^i} \quad (r = 1, \ldots, 6). \tag{16}$$

(b) The linearization partial velocity of the slider is

$$\overset{S_i}{}_l \vec{v}_r^{A_i^*} = \frac{\partial \overset{S_i}{}_l \vec{v}^{A_i^*}}{\partial u_r^i} \quad (r = 1, \ldots, 6). \tag{17}$$

(c) The linearization partial velocity of scientific platform is

$$\overset{S_1}{}_l \vec{v}_r^{F^*} = \frac{\partial \overset{S_1}{}_l \vec{v}^{F^*}}{\partial u_r^i} \quad (r = 1, \ldots, 6). \tag{18}$$

Define $\widehat{M_i}$ and $\widehat{N_i}$ as the coordinating system during the relative rotation between $\widehat{F_i}$ and $\widehat{A_i}$; $\widehat{K_i}$ is that between $\widehat{P_i}$ and $\widehat{S_i}$. Thus, the generalized angular velocities are

$$^{F_i}\vec{\omega}^{M_i} = u_1^i \vec{f}_1^i, \tag{19}$$
$$^{M_i}\vec{\omega}^{N_i} = u_2^i \vec{m}_2^i, \tag{20}$$
$$^{N_i}\vec{\omega}^{A_i} = u_3^i \vec{n}_3^i, \tag{21}$$
$$^{P_i}\vec{\omega}^{A_i} = 0, \tag{22}$$

$$^{K_i}\vec{\omega}^{P_i} = u_6^i \vec{k}_3^i \tag{23}$$

$$^{S_i}\vec{\omega}^{K_i} = u_5^i \vec{s}_1^i. \tag{24}$$

Then, the angular velocity of the rigid is obtained by superposition principle:

$$^{S_i}\vec{\omega}^{P_i} = u_5^i \vec{s}_1^i + u_6^i \vec{k}_3^i, \tag{25}$$

$$^{S_i}\vec{\omega}^{A_i} = u_5^i \vec{s}_1^i + u_6^i \vec{k}_3^i, \tag{26}$$

$$^{S_1}\vec{\omega}^{F} = u_5^1 \vec{s}_1^1 + u_6^1 \vec{k}_3^1 - u_1^1 \vec{f}_1^1 - u_2^1 \vec{m}_2^1 - u_3^1 \vec{n}_3^1. \tag{27}$$

The angular accelerations of rigid elements are derived by the time derivatives of angular velocities after linearization, which are obtained as follows:

$$^{S_i}\vec{\alpha}^{P_i} = \dot{u}_5^i \vec{s}_1^i + \dot{u}_6^i \vec{k}_3^i, \tag{28}$$

$$^{S_i}\vec{\alpha}^{A_i} = \dot{u}_5^i \vec{s}_1^i + \dot{u}_6^i \vec{k}_3^i, \tag{29}$$

$$^{S_1}\vec{\alpha}^{F} = \dot{u}_5^1 \vec{s}_1^1 + \dot{u}_6^1 \vec{k}_3^1 - \dot{u}_1^1 \vec{f}_1^1 - \dot{u}_2^1 \vec{m}_2^1 - \dot{u}_3^1 \vec{n}_3^1. \tag{30}$$

Then, the partial angular velocities after linearization are obtained as follows.

(a) The partial angular velocity of the static lever after linearization is

$$^{S_i}_{l}\vec{\omega}_r^{P_i} = \frac{\partial_l^{S_i}\vec{\omega}^{P_i}}{\partial u_r^i} \quad (r = 1, \ldots, 6). \tag{31}$$

(b) The partial angular velocity of the slider after linearization is

$$^{S_i}_{l}\vec{\omega}_r^{A_i} = \frac{\partial_l^{S_i}\vec{\omega}^{A_i}}{\partial u_r^i} \quad (r = 1, \ldots, 6). \tag{32}$$

(c) The partial angular velocity of the scientific platform after linearization is

$$^{S_1}_{l}\vec{\omega}_r^{F} = \frac{\partial_l^{S_1}\vec{\omega}^{F}}{\partial u_r^1} \quad (r = 1, \ldots, 6). \tag{33}$$

3.4 Generalized active force and generalized inertia force

The main disturbance is the force and moment imposed on the scientific platform directly and accompanied by the moment via deformation of flexure hinge, which is from the joint of 3-DOF flexure hinge aforementioned. The resultant moment of all the eight joints is

$$\vec{M}^F = \sum_{i=1}^{8} \left(k_1^i q_1^i \vec{f}_1^i + k_2^i q_2^i \vec{m}_2^i + k_3^i q_3^i \vec{n}_3^i \right). \tag{34}$$

The force and moment of disturbances imposed directly on the centroid of mass of science platform will be defined as $\vec{F}^D$ and $\vec{M}^D$, repectively.

The generalized active force for generalized velocity of the i-th rigid body is:

$$_l Q_r^F = {}^{S_1}_{l}\vec{v}_r^{F^*} \cdot \vec{F}^D + {}^{S_1}_{l}\vec{\omega}_r^F \cdot \left(\vec{M}^D + \vec{M}^F \right). \tag{35}$$

Force and moment imposed on slider include the pushing force and deforming moments from flexure hinge.

The pushing force imposed on position A_i is defined as $\vec{F}^{C_i}$, where c is the ratio of damping.

$$\vec{F}^{C_i} = \left(F^{C_i} - c u_4^i \right) \vec{a}_2^i. \tag{36}$$

Let $\vec{M}^{F_i}$ be the deforming moment for the i-th slider, which can be derived as:

$$-\vec{M}^{F_i} = -\left(k_1^i q_1^i \vec{f}_1^i + k_2^i q_2^i \vec{m}_2^i + k_3^i q_3^i \vec{n}_3^i \right). \tag{37}$$

Thus, the generalized active force of generalized velocity for the r-th slider is represented as

$$_l Q_r^{A_i} = {}^{S_i}_{l}\vec{v}_r^{A_i^*} \cdot \vec{F}^{C_i} + {}^{S_i}_{l}\vec{\omega}_r^{A_i} \cdot \left(-\vec{M}^{F_i} \right). \tag{38}$$

As aforementioned, forces and moments imposed on static lever include pushing force of the voice coil motor and moment of flexure hinge deformation. Define that $\vec{M}^{S_i}$ represents the resultant moment, which is derived by

$$\vec{M}^{S_i} = k_5^i q_5^i \vec{s}_1^i + k_6^i q_6^i \vec{k}_3^i. \tag{39}$$

The generalized active force for the generalized velocity of r-th rigid body is:

$$_l Q_r^{P_i} = {}^{S_i}_{l}\vec{v}_r^{P_i^*} \cdot \left(-\vec{F}^{C_i} \right) + {}^{S_i}_{l}\vec{\omega}_r^{P_i} \cdot \vec{M}^{S_i}. \tag{40}$$

Define m_F, m_{A_i}, and m_{P_i} as the masses of scientific platform, the slider, and the static lever, respectively. Moreover, their inertia moments are J_F, J_{A_i}, and J_{P_i}.

The generalized inertia force according to the r-th generalized velocity of the scientific platform is

$$\left({}_l Q_r^*\right)^F = {}_l^{S_1}\vec{v}_r^{F^*} \cdot \left[-m_F \left({}_l^{S_1}\vec{a}^{F^*} + \vec{a}^S\right)\right] + {}_l^{S_1}\vec{\omega}_r^F \cdot \left[-J_F {}^{S_1}\vec{\alpha}^F - {}^{S_1}\vec{\omega}^F \times \left(J_F {}^{S_1}\vec{\omega}^F\right)\right]. \tag{41}$$

Then, the generalized inertia forces according to the r-th generalized velocities of the slider and the static lever are

$$\left({}_l Q_r^*\right)^{A_i} = {}_l^{S_i}\vec{v}_r^{A_i^*} \cdot \left[-m_{A_i} \left({}_l^{S_i}\vec{a}^{A_i^*} + \vec{a}^S\right)\right] + {}_l^{S_i}\vec{\omega}_r^{A_i} \cdot \left[-J_{A_i} {}^{S_i}\vec{\alpha}^{A_i} - {}^{S_i}\vec{\omega}^{A_i} \times \left(J_{A_i} {}^{S_i}\vec{\omega}^{A_i}\right)\right], \tag{42}$$

$$\left({}_l Q_r^*\right)^{P_i} = {}_l^{S_i}\vec{v}_r^{P_i^*} \cdot \left[-m_{P_i} \left({}_l^{S_i}\vec{a}^{P_i^*} + \vec{a}^S\right)\right] + {}_l^{S_i}\vec{\omega}_r^{P_i} \cdot \left[-J_{P_i} {}^{S_i}\vec{\alpha}^{P_i} - {}^{S_i}\vec{\omega}^{P_i} \times \left(J_{P_i} {}^{S_i}\vec{\omega}^{P_i}\right)\right]. \tag{43}$$

3.5 Dynamics equations

There are totally 48 kinematic equations, each of which is in accordance with a coordinate system as:

$$u_j^i = \dot{q}_j^i \quad (j = 1, \ldots, 6;\ i = 1, \ldots, 8). \tag{44}$$

Moreover, there are 6 equations of dynamics, each one is in accordance with a generalized velocity linearization independence.

With the analysis of the dynamics system for $\tilde{S}$, which includes 17 rigid bodies in all, the generalized active force is:

$$F_r = {}_l Q_r^F + \sum_{i=1}^{8} {}_l Q_r^{A_i} + \sum_{i=1}^{8} {}_l Q_r^{P_i}. \tag{45}$$

Then, the generalized inertia force is:

$$F_r^* = \left({}_l Q_r^*\right)^F + \sum_{i=1}^{8} \left({}_l Q_r^*\right)^{A_i} + \sum_{i=1}^{8} \left({}_l Q_r^*\right)^{P_i}. \tag{46}$$

As the dependent generalized velocity is represented by a linear combination of the generalized velocities with linear independence,

$$u_j^i = \sum_{j=1}^{6} A_{rj} u_j^1 + B_r \times (i = 2, \ldots, 8;\ j = 1, \ldots, 6;\ r = 7, \ldots, 48). \tag{47}$$

With the same method, the generalized active force and the generalized inertia force are as follows:

$$\tilde{F}_j = F_j + \sum_{r=7}^{48} A_{rj} F_j \quad (j = 1, \ldots, 6), \tag{48}$$

$$\tilde{F}_j^* = F_j^* + \sum_{r=7}^{48} A_{rj} F_j^* \quad (j = 1, \ldots, 6). \tag{49}$$

Based on Kane's dynamic equation:

$$\tilde{F}_j + \tilde{F}_j^* = 0 \quad (j = 1, \ldots, 6) \tag{50}$$

According to Kane's method, the kinetic model of the system can be written in the following state-space form [4,8]

$$\underbrace{\begin{bmatrix} I & O & O \\ O & I & O \\ O & O & M \end{bmatrix}}_{P} \underbrace{\begin{Bmatrix} \dot{\vec{q}}^I \\ \dot{\vec{q}}^D \\ \dot{\vec{u}}^I \end{Bmatrix}}_{\dot{\vec{x}}} = \underbrace{\begin{bmatrix} O & O & I \\ O & O & N \\ K_i & K_d & C \end{bmatrix}}_{A} \underbrace{\begin{Bmatrix} \vec{q}^I \\ \vec{q}^D \\ \vec{u}^I \end{Bmatrix}}_{\vec{x}} + \begin{bmatrix} O \\ O \\ B \end{bmatrix} \left\{\vec{f}\right\} + \begin{bmatrix} O \\ O \\ D \end{bmatrix} \left\{\vec{d}\right\}. \tag{51}$$

In (51), $\vec{x}$, $\vec{f}$, and $\vec{d}$ represent the status, the inputs, and the disturbance, respectively. I and O are unit matrix and zero matrix, respectively. P, A and D are definite matrices. B is the linear combination of the state quantity, and B is time-varying matrix.

State variables consist of 48 generalized coordinates $\vec{x}$ and 6 independent generalized velocities $\vec{u}^I$, as

$$\vec{q}^I = \left[q_1^1\ q_2^1\ q_3^1\ q_4^1\ q_5^1\ q_6^1\right]^T, \tag{52}$$

where $\vec{q}^I$ is a 6×1 matrix, which represents 6 generalized coordinates of the actuator i, which are five rotations between two flexure hinge and a displacement generated in sliding pair.

$$\vec{q}^D = \left[q_1^i\ q_2^i\ q_3^i\ q_4^i\ q_5^i\ q_6^i\right]^T, \quad (i = 2, \ldots, 8), \tag{53}$$

where $\vec{q}^D$ is a 42×1 matrix, and it represents all the rotations and displacements of actuators 2 to 8.

$$\vec{u}^I = \left[u_1^1\ u_2^1\ u_3^1\ u_4^1\ u_5^1\ u_6^1\right]^T, \tag{54}$$

where $\vec{u}^I$ is a 6×1 matrix, which is the first-order derivative of the generalized coordinate system for actuator i.

Input variable $\vec{f}$ is a 8×1 matrix, which represents the driving force of eight actuators. Force is acted

between the slide and the static lever. Disturbance variable $\vec{d}$ is a 6×1 matrix, which represents 3 disturbance forces and 3 disturbances torques, respectively. Disturbance force acts on the centroid position of the experimental platform.

N is a 42×6 definite matrix, which is composed of the geometric parameters of the system. Twenty-one equations represent that it should be the same on values of scientific experimental platform's centroid velocity in different coordinate systems. Another 21 equations represent that it should be the same on values of scientific experimental platform's angular velocity in different coordinate systems.

$$ {}^{S_1}_{l}\vec{v}^{F^*} = {}^{S_i}_{l}\vec{v}^{F^*} \quad (i = 2, \ldots, 8), \tag{55} $$

$$ {}^{S_1}_{l}\vec{\omega}^{F} = {}^{S_i}_{l}\vec{\omega}^{F} \ (i = 2, \ldots, 8) \tag{56} $$

M is a 6×6 matrix, composed of quality and inertia of scientific experimental platform, eight sliders, and eight levers, which is a definite matrix.

K_i and K_d are stiffness matrices, composed of stiffness of 16 flexible hinges, which are definite matrices.

4 Checking of controllability and observability

In control theory, both controllability and observability are two critical properties for a control system, and the controllability plays a crucial role in control problems, such as stabilization of unstable system by feedback, while observability measures how well internal states of a system can be inferred by knowledge of its external outputs.

Considering the model proposed, the state-space equation is given by

$$ \begin{cases} \dot{x} = Ax + B_1\omega + B_2u \\ y = Cx + D_1\omega + D_2u \end{cases}, \tag{57} $$

where x is a 12×1 state vector, which equals to $\left[q^I \ u^I \right]^T$, y is a 12×1 output vector, which equals to $\left[r^{F^*} \ \theta^{F^*} \ a^{F^*} \ \alpha^{F^*} \right]^T$.

When the payload of the system is at balance position and at initial time, as $y = O_{12\times1}$; r^{F^*} and θ^{F^*} are the shift and angle of the payload with respect to the initial position.

Considering that $u = [Bf]$ is the 6×1 input vector and $\omega = [d]$ is the 6×1 disturbance vector, we can derive

$$ A = \begin{bmatrix} O_{6\times6} & I_{6\times6} \\ -\frac{K_i + K_d N}{M}_{6\times6} & -\frac{C}{M}_{6\times6} \end{bmatrix}_{12\times12}, \tag{58} $$

$$ B_1 = \begin{bmatrix} O_{6\times6} \\ -\frac{D}{M}_{6\times6} \end{bmatrix}_{12\times6}, \tag{59} $$

$$ B_2 = \begin{bmatrix} O_{6\times6} \\ -\frac{I}{M}_{6\times6} \end{bmatrix}_{12\times6}, \tag{60} $$

$$ y = \begin{bmatrix} \begin{pmatrix} {}^{S_1}_{l}\vec{v}_1^{F^*} & \cdots & {}^{S_1}_{l}\vec{v}_6^{F^*} \end{pmatrix} & O \\ \begin{pmatrix} {}^{S_1}_{l}\vec{\omega}_1^{F} & \cdots & {}^{S_1}_{l}\vec{\omega}_6^{F} \end{pmatrix} & O \\ O & \begin{pmatrix} {}^{S_1}_{l}\vec{v}_1^{F^*} & \cdots & {}^{S_1}_{l}\vec{v}_6^{F^*} \end{pmatrix} \\ O & \begin{pmatrix} {}^{S_1}_{l}\vec{\omega}_1^{F} & \cdots & {}^{S_1}_{l}\vec{\omega}_6^{F} \end{pmatrix} \end{bmatrix}_{12\times12} $$

$$ \times \begin{bmatrix} q_1 \\ \vdots \\ q_6 \\ \dot{u}_1 \\ \vdots \\ \dot{u}_6 \end{bmatrix} = \begin{bmatrix} F & O \\ O & F \end{bmatrix} \begin{bmatrix} q_1 \\ \vdots \\ q_6 \\ \dot{u}_1 \\ \vdots \\ \dot{u}_6 \end{bmatrix}, \tag{61} $$

$$ C = \begin{bmatrix} K_{6\times6} & O_{6\times6} \\ -\frac{F(K_i + K_d N)}{M}_{6\times6} & -\frac{FC}{M}_{6\times6} \end{bmatrix}_{12\times12}, \tag{62} $$

$$ D_1 = \begin{bmatrix} O_{6\times6} \\ -\frac{FD}{M}_{6\times6} \end{bmatrix}_{12\times6}, \tag{63} $$

$$ D_2 = \begin{bmatrix} O_{6\times6} \\ -\frac{F}{M}_{6\times6} \end{bmatrix}_{6\times6}. \tag{64} $$

The controllability matrix of the system is given by:

$$ U_c = \left[B_2 \ AB_2 \cdots A^{11}B_2 \right]. \tag{65} $$

The observability matrix of the system is given by:

$$ U_o = \left[C \ CA \cdots CA^{11} \right]^T. \tag{66} $$

The system is controllable and observable if the controllability and observability matrices have full rank. Thus, those of the system proposed are calculated as

$$ \text{rank}(U_c) = \text{rank}(x) = 12, $$
$$ \text{rank}(U_o) = \text{rank}(x) = 12. $$

Based on the analysis method aforementioned and the results above, there is sufficient evidence to draw the conclusions that the system proposed is controllable and observable.

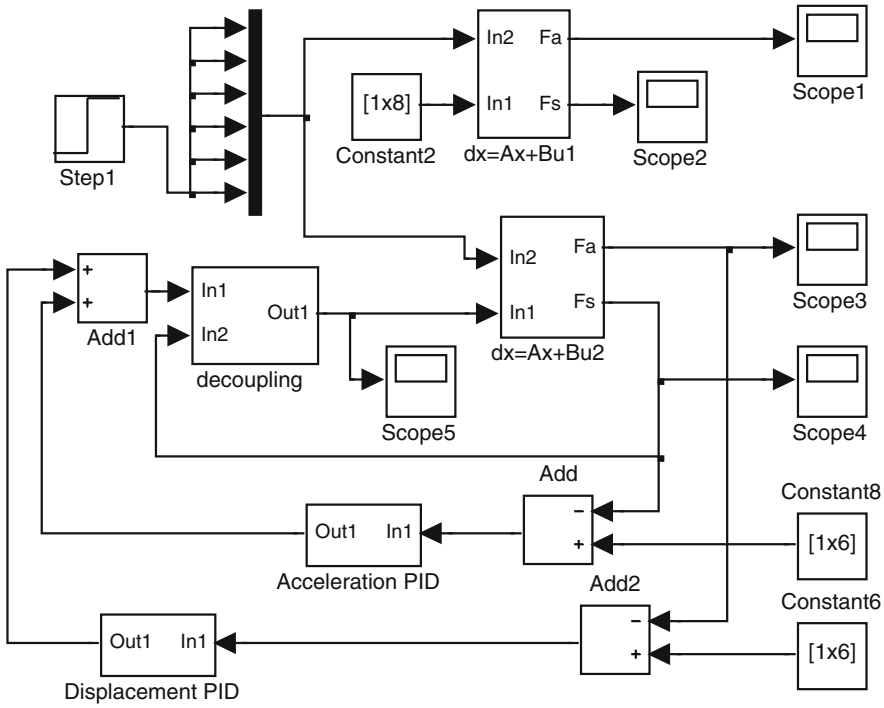

Fig. 4 A PID control block diagram

5 PID control and simulation

Referring to the control methods introduced in [16,17], the control diagram of the proposed system is shown in Fig. 4, which includes both open-loop and closed-loop strategies. The controller is composed of the feedback decoupled controller and the double-loop feedback PID controller including both position and acceleration. The input of open-loop system is disturbance force, while the voice coil motor will not work. The inputs of closed-loop system are disturbance force and the acting force controlled by feedback.

Each feedback of acceleration and position constructs an independent PID controller. After decoupled, each controller is designed independently with classical control methods for attenuating the disturbance of single DOF.

Decoupling controller is shown as Fig. 5, which includes decoupling matrix of mass M^*, decoupling matrix of stiffness K^*, and acting force distribution matrix B^*. Here,

$$M^* = M,\ B^*B = I,\ K^* - (K_i + K_d N) = K', \quad (67)$$

where K' is the diagonal elements in matrix $K_i + K_d N$.

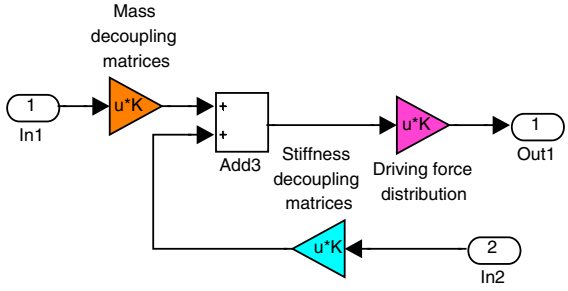

Fig. 5 A decoupled controller

The responses for unit step disturbance in six degrees of freedom are shown in Figs. 6 and 7. From the simulation results in the figures, it is noticed that there is a large vibration with open-loop controller in the form of acceleration and displacement of centroid. The result of acceleration and angular of load's centroid of the closed-loop system are shown in Fig. 8, while the displacement and angle of payload are shown in Fig. 9. Comparing with the results of open-loop controller, both the acceleration and displacement of position and angular are reduced significantly. The amplitude of the acceleration $a^{F^*}_{\text{closed}}$ and the angular acceleration $\alpha^{F^*}_{\text{closed}}$ are no larger than 5×10^{-12}, and the amplitude of the acceleration $r^{F^*}_{\text{closed}}$ and the angular acceleration $\theta^{F^*}_{\text{closed}}$

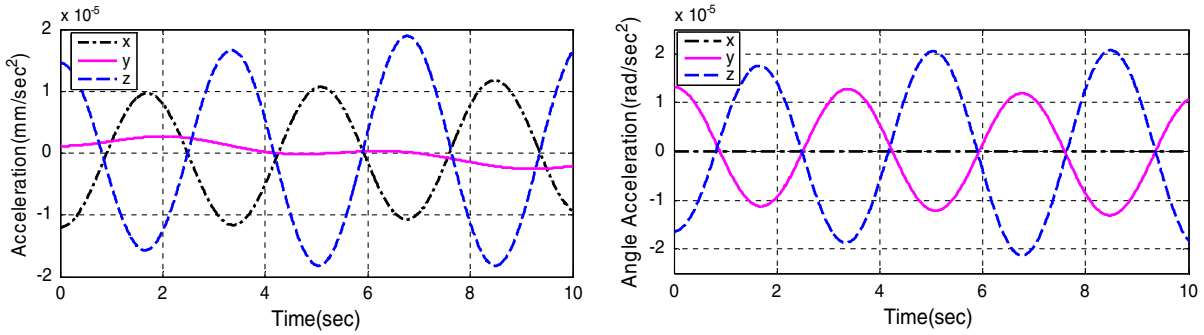

Fig. 6 Acceleration and angle acceleration of payload center-of-mass in open-loop system

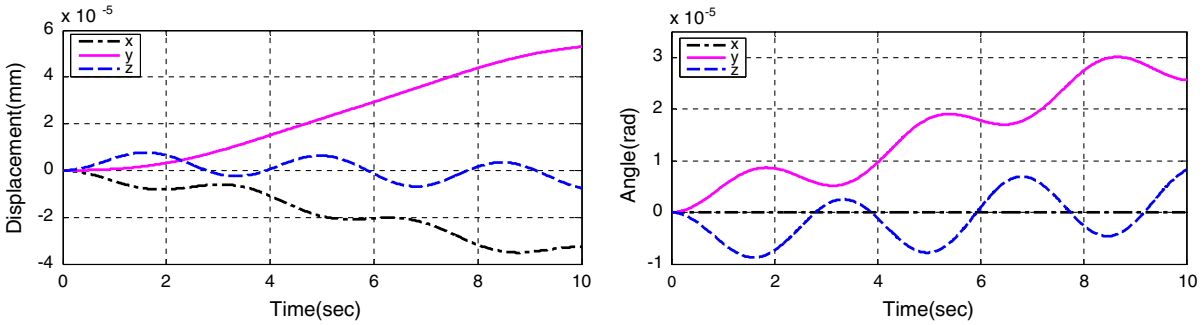

Fig. 7 Displacement and angle of payload center-of-mass in open-loop system

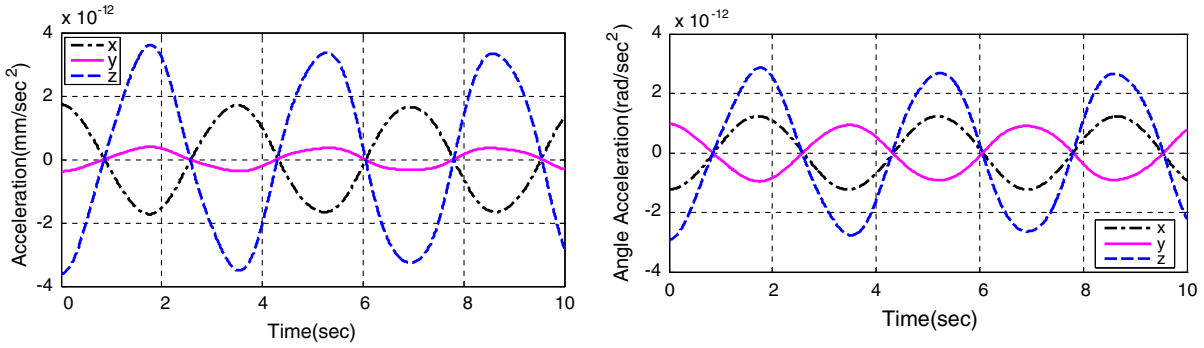

Fig. 8 Acceleration and angle acceleration of payload center-of-mass in closed-loop system with PID controller

are no larger than 2.5×10^{-10}. Table 1 shows the magnitude of the acceleration and magnitude of the displacement of the open-loop system and active vibration isolation system with PID controller at some of the time point.

From simulation experiment we can see that acceleration and displacement at centroid of experimental load both were obtained with excellent attenuation and can restrain vibration that is caused by disturbance force. But PID control belongs to the classic controlling method, which is used for MIMO system requiring adequate decoupling as a precondition. The design of decoupling controller relies on the accurate measurement of the mass matrix and the stiffness matrix and it cannot be fully decoupled because of the presence of system damping. If the system's damping is great, the effect of decoupling will be affected to some degree (Fig. 10).

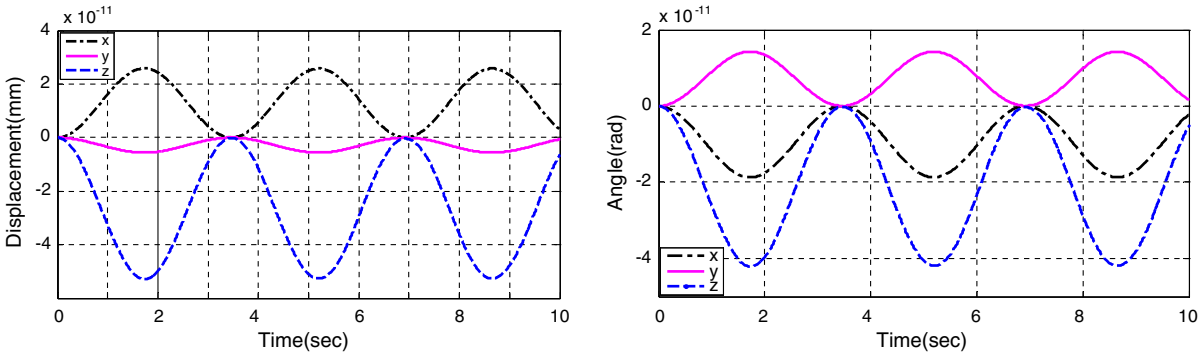

Fig. 9 Displacement and angle of payload center-of-mass in closed-loop system with PID controller

Table 1 Vibration isolation effect of parallel active vibration isolation system by PID control

Time (s)	Combined acceleration (mm/s^2)		Combined angular acceleration (rad/s^2)		Combined displacement (mm)		Combined corner (rad)	
	Open Loop	PID control	Open Loop	PID control	Open Loop	PID control	Open Loop	PID control
5	1.34e−5	5.02e−13	1.22e−5	3.47e−13	9.02e−6	1.49e−11	6.71e−6	1.79e−11
10	8.25e−6	4.66e−13	1.04e−5	2.68e−13	1.26e−6	2.76e−11	1.04e−5	2.48e−10
15	1.11e−5	2.79e−13	1.36e−5	1.07e−13	6.71e−6	4.01e−11	3.21e−5	4.07e−10
20	1.02e−5	1.38e−13	1.17e−5	8.28e−14	2.92e−6	5.28e−11	5.44e−6	6.11e−10

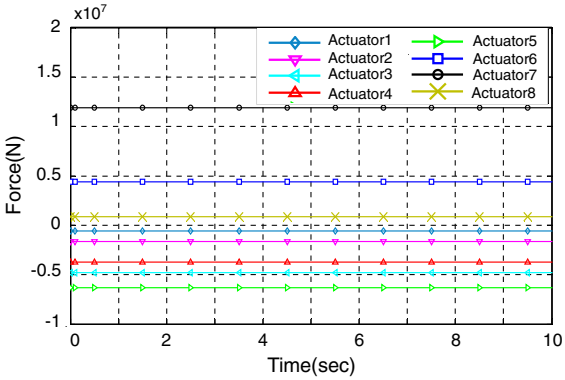

Fig. 10 Driving forces of voice coil actuators

6 H_∞ control and simulation

Modern control method is more suitable for MIMO system control; according to H_∞ control method, the state equation of control system is modern control method and it is more suitable for MIMO system control.

$$\begin{cases} \dot{x} = Ax + B_1\omega + B_2u \\ z = C_1x + D_{12}u \\ y = C_2x + D_{21}\omega + D_{22}u \end{cases}, \tag{68}$$

where x is the state vector, ω is the disturbance vector, u is the control vector, z is the reference output vector, and y is the output vector.

At the initial state, $x(0) = O_{12\times1}$; while for any interference loop system, it should have the ability to suppress disturbances, namely

$$\int_0^\infty \left(\sum_{i=1}^{6} k_i q_i^l + \sum_{i=1}^{6} m_i \dot{u}_i^l + \sum_{i=1}^{8} n_i f_i \right) \mathrm{d}t < \int_0^\infty \omega, \tag{69}$$

where $k_i \geq 0$, $m_i \geq 0$, $i = (1, \ldots, 6)$, and $n_i > 0$ $(i = 1, \ldots, 8)$ are weighting factors. Weighting coefficients are $k_i = 100$, $m_i = 10^8$, and $n_i = 1$.

Evaluation signal is defined as

$$z = C_1x + D_{12}u. \tag{70}$$

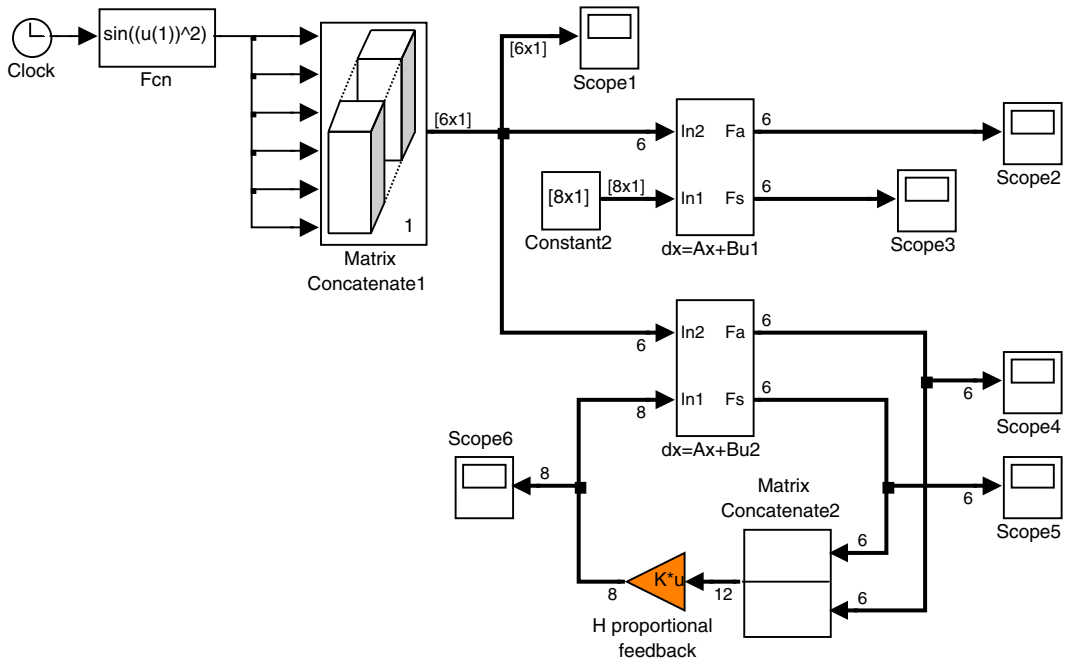

Fig. 11 H_∞ control block diagram

Here,

$$C_1 = \begin{bmatrix} \begin{pmatrix} \sqrt{k_1} & & \\ & \ddots & \\ & & \sqrt{k_6} \end{pmatrix}_{6\times 6} & \begin{pmatrix} \sqrt{m_1} & & \\ & \ddots & \\ & & \sqrt{m_6} \end{pmatrix}_{6\times 6} \\ \begin{pmatrix} 0 & & \\ & \ddots & \\ & & 0 \end{pmatrix}_{8\times 6} & \begin{pmatrix} 0 & & \\ & \ddots & \\ & & 0 \end{pmatrix}_{8\times 6} \end{bmatrix}_{20\times 12} \tag{71}$$

$$D_{12} = \begin{bmatrix} \begin{pmatrix} 0 & & \\ & \ddots & \\ & & 0 \end{pmatrix}_{12\times 8} \\ \begin{pmatrix} \sqrt{n_1} & & \\ & \ddots & \\ & & \sqrt{n_8} \end{pmatrix}_{8\times 8} \end{bmatrix}_{20\times 8}. \tag{72}$$

Thus,

$$\|z\|_2 < \|\omega\|_2 . \tag{73}$$

For the existing status feedback $u = -Kx$, which can make the control system stable, the necessary and sufficient condition of $\|z\|_2 < \|\omega\|_2$ is the Riccati equation.

$$A^T P + PA + P\left(B_1 B_1^T - B_2 B_2^T\right) + C_1^T C_1 = 0. \tag{74}$$

There is semi-definite solution ($P \geq 0$) that can make $A + \left(B_1 B_1^T - B_2 B_2^T\right) P$ stable. If we find the positive definite solution P of the Riccati equation, the feedback matrix is

$$K = B_2^T P, \tag{75}$$

Control block diagram is shown as Fig. 11, it also includes open-loop system and the closed-loop system with a feedback controller. The input of open-loop system is disturbance and the voice coil motors are turned off in this situation. The inputs of closed-loop system are disturbance force and the driving force of the feedback control as shown in Fig. 12.

We can get acceleration and angular of centroid of open-loop system as shown in Fig. 13, and displacement and angle as shown in Fig. 14. The amplitude of the acceleration $a_{\text{open}}^{F^*}$ and the angular acceleration $\alpha_{\text{open}}^{F^*}$ will not exceed 5×10^{-5}. The amplitude of the acceleration $r_{\text{open}}^{F^*}$ and the angular acceleration $\theta_{\text{open}}^{F^*}$ will not exceed 1×10^{-5}.

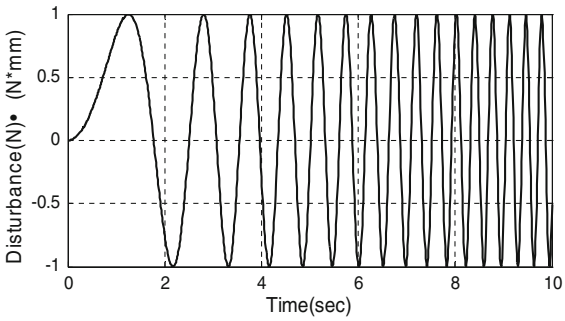

Fig. 12 Disturbance forces

We can get acceleration and angular of centroid of closed-loop system as shown in Fig. 15, and displacement and angle as shown in Fig. 16. The amplitude of the acceleration a^{F*}_{closed} and the angular acceleration $\alpha^{F*}_{\text{closed}}$ will not exceed 4×10^{-12}. The amplitude of the acceleration r^{F*}_{closed} and the angular acceleration $\theta^{F*}_{\text{closed}}$ will not exceed 2×10^{-11}.

The acting forces of eight voice coil motors are shown in Fig. 17, the maximum output of which is no larger than 2×10^4N.

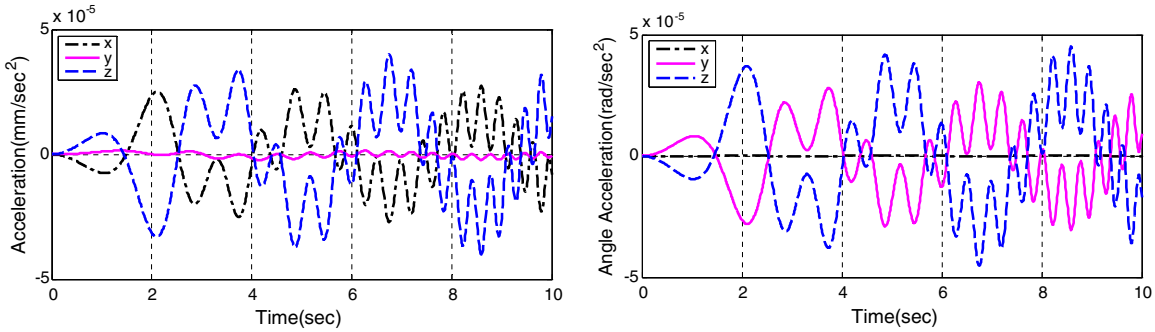

Fig. 13 Acceleration and angle acceleration of payload center-of-mass in open-loop system under disturbance forces

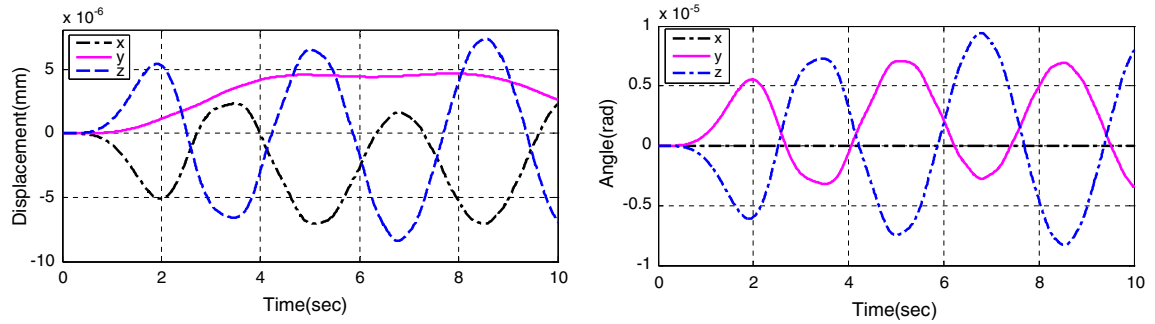

Fig. 14 Displacement and angle of payload center-of-mass in open-loop system under disturbance forces

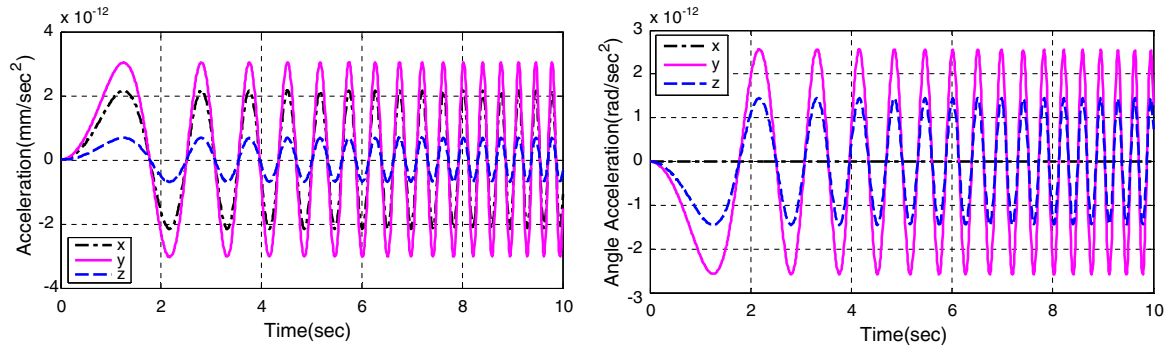

Fig. 15 Acceleration and angle acceleration of payload center-of-mass in closed-loop system with H_∞ controller

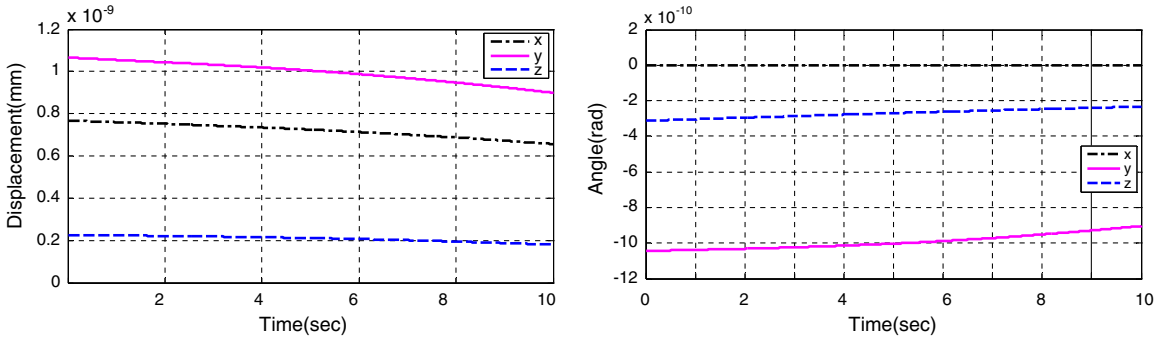

Fig. 16 Displacement and angle of payload center-of-mass in closed-loop system with H_∞ controller

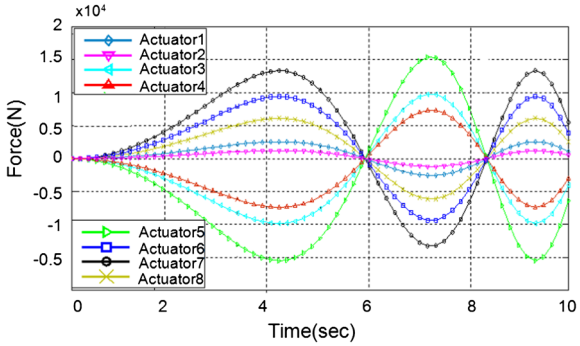

Fig. 17 Driving forces of voice coil actuators

The effectiveness of the proposed active damping system with H_∞ control law is listed in Table 2, which shows the amplitudes of acceleration and displacement of both open-loop and closed-loop with H_∞ control law. The above results demonstrate that the proposed system with H_∞ control law is effective for isolation application by attenuating the vibration and it is even better than that with the PID controller aforementioned. We will perform an experimental study on the fabricated prototype in the next step of work [18].

7 Conclusion

The proposed active vibration isolation prototype is a typical MIMO system utilizing eight voice coil motors as the single-axis isolation to attenuate the acceleration and displacement of science research platform during disturbances. In this paper, the system's characteristics are analyzed and the state-space equations of the system are also obtained. Then, the controllability and observability of the system are analyzed. Moreover, the classical control method and the modern control method are used to design a dual feedback controller. The decoupling method is used to make each channel of feedback signal independent with each other. Then for each channel, a PID controller is designed individually. With the modern control method, H_∞control law is adopted and the feedback matrix is designed according to state-space equations. From the simulation results, both PID control and H_∞ control

Table 2 Vibration isolation effect of parallel active vibration isolation system by H_∞ control

Time(s)	Combined acceleration (mm/s^2)		Combined angular acceleration (rad/s^2)		Combined displacement (mm)		Combined corner (rad)	
	Open loop	H_∞ control	Open loop	H_∞ control	Open loop	H_∞ control	Open loop	H_∞ control
5	9.79e−6	2.03e−12	1.61e−5	2.20e−12	4.56e−6	6.20e−12	7.08e−6	4.20e−12
10	1.27e−5	1.54e−12	6.83e−6	1.67e−12	2.49e−6	1.26e−11	3.60e−6	6.25e−12
15	2.24e−5	2.44e−12	2.24e−5	2.52e−12	3.97e−6	1.94e−11	1.94e−6	1.94e−11
20	1.16e−5	1.69e−12	2.40e−6	1.43e−12	4.84e−6	3.23e−11	6.92e−6	2.26e−11

laws are effective for attenuating the acceleration and displacement.

Acknowledgments This research is supported by the National Natural Science Foundation of China (51175494 and 61128008), the State Key Laboratory of Robotics Fund (O8A120S), and Macao Science and Technology Development Fund (108/2012/A3).

References

1. Li, Z.F., Ren, W.J.: Study on active vibration isolation technology of space microgravity. Manned Spacefl. **16**(3), 24–32 (2010)
2. Yu, Q., Jin, D.R.: Introduction to the theory and examples of the microgravity vibration isolation system. Manned Spacefl. **3**, 16–18 (2008)
3. Grodsinsky, C.M., Whorton, M.S.: Survey of active vibration isolation systems for microgravity applications. J. Spacecr. Rocket. **37**(5), 586–596 (2000)
4. Hampton, R.D., Beech, G.A.: "Kane's Dynamics" Model for the Active Rack Isolation System. NASA/TM-2005-213848, Marshall Space Flight Center, Huntsville (2005)
5. Bushnell, G. S., Anderson, T.M., Becraft, M.D., Jacot A.: Active rack isolation system development for the International Space Station. AIAA 1997–1203 (1997)
6. Bushnell, G.S., Becraft, M.D.: Microgravity performance flight characterization of an international space station active rack isolation prototype system. In: Proceedings of the 16th IEEE Instrumentation and Measurement Technology Conference, pp. 260–267 (1999)
7. Hampton, R.D., Nagendra, N., Subba, R.: A high-fidelity dynamic model for the active rack isolation system. AIAA-98-0458 (1998)
8. Hampton, R.D., Naveed, Q.: A state-space model of ARIS for optimal controller design: MATLAB implementation. AIAA 2004–786 (2004)
9. Beech, G.S., Hampton, R.D.: A simplified model of ARIS for optimal controller design. AIAA-2001-1138 (2001).
10. Beech, G.S., Hampton, R.D.: Validation of a "Kane's dynamics" model for the active rack isolation system. AIAA-2000-16541 (2000)
11. Yun, Y., Li, Y.: Modeling and control analysis of a 3-PUPU dual compliant parallel manipulator for micro positioning and active vibration isolation. J. Dyn. Syst. Meas. Control Trans. ASME **134**(2), 021001-1-9 (2012)
12. Yun, Y., Li, Y.: Design and analysis of a novel 6-DOF redundant actuated parallel robot with compliant hinges for high precision positioning. Nonlinear Dyn. **61**(4), 829–845 (2010)
13. Li, Y., Staicu, S.: Inverse dynamics of a 3-PRC parallel kinematic machine. Nonlinear Dyn. **67**(2), 1031–1041 (2012)
14. Li, Y., Liu, Y., Liu, X.: Active vibration control of a modular robot combining a BP neural network with a genetic algorithm. J. Vib. Control **11**(1), 3–17 (2005)
15. Yun, Y., Li, Y.: A general dynamics and control model of a class of multi-DOF manipulators for active vibration control. Mech. Mach. Theory **46**(10), 1549–1574 (2011)
16. Bushnell, G.S., Anderson, T.M., Becraft, M.D., Jacot, A.D.: Active rack isolation system development for the International Space Station. In: The 38th Structures, Structural Dynamics, and Materials Conference, 7–10 April, pp. 1500–1506 (1997)
17. Bushnell, G.S., Becraft, M.D.: Microgravity performance flight characterization of an International Space Station active rack isolation prototype system. In: Proceedings of the 16th IEEE Instrumentation and Measurement Technology Conference, pp. 260–267 (1999)
18. Laalej, H., Lang, Z.Q., Daley, S., Zazas, I., Billings, S.A., Tomlinson, G.R.: Application of non-linear damping to vibration isolation: an experimental study. Nonlinear Dyn. **69**(1), 409–421 (2012)